Optica Applicata, Vol. LII, No. 4, 2022
DOI: 10.37190/oa220414

Numerical analysis of slow and fast light effect in semiconductor optical amplifier with certain facet reflection

CUI QIN*, YU JIANG, LI ZHEN

School of Information and Communication Engineering, Nanjing Institute of Technology, Nanjing 211167, China

*Corresponding author: qincui@njit.edu.cn

In this paper, the slow and fast light (SFL) effects of the semiconductor optical amplifier (SOA) having certain facet reflections are theoretically investigated. The theoretical model is used to account for the SFL phenomenon causing the coherent population oscillation. The influence of the current modulation frequency, the value of the current, the linewidth enhancement factor, facet reflectivity as well as the relative phase of the modulated current on the phase delay in the SOA are studied. It is demonstrated that the SFL effect could be controlled by the modulation frequency, the value and relative phase of the current. Finally, it is shown that the magnitude of the SFL delay could be tuned by a change in the linewidth enhancement factor as well as the facet reflectivity of the SOA.

Keywords: semiconductor optical amplifiers, slow and fast light, coherent population oscillation.

1. Introduction

Semiconductor optical amplifiers (SOAs) have a wide range of applications in all-optical signal processing technologies of next-generation optical networks for advantages such as various nonlinearities, direct current pumping, wide operational range, and small footprint [1,2]. However, the nonlinearity is limited to the processing of high-speed signals, which is a disadvantage for SOA-based applications. Methods for improving the nonlinearity of the SOAs have gathered much attention [3,4]. Several methods have been proposed to alleviate this problem. For instance, a variety of structures, such as the quantum dot, multiple quantum wells, and varying composition quantum wells, which have different material gain spectrum, refractive index, and differential gain properties, were used for fabricating the SOAs. Other measures concentrate on improving the nonlinearity by introducing slow light in the semiconductor medium [5,6]. Slow light is the propagation of an optical pulse at a very low group velocity. Slow light occurs when the pulse propagation is slowed down due to the interaction with the medium.

Currently, there are two approaches to slow light generation: one uses dispersion which finds an optimal structure that enhances the nonlinear response through geometric properties; the other uses nonlinear optical effects such as electromagnetic induction transparency, coherent population oscillation, Raman, and Brillouin amplification [7,8]. In this paper, the phenomenon of slow and fast light (SFL) generation is analyzed using coherent population oscillation in SOAs. Coherent population oscillation is powerful physical mechanism which allows for the variation of group velocity. Coherent population oscillation produces a narrow hole in the gain spectra as a consequence of the periodic modulation of the carrier density at the beat frequency between a control field and a probe field. SFL at room temperature can be achieved in semiconductor quantum wells and quantum dots [9].

A theoretical model is constructed based on the coherent population oscillation effect within a facet-reflective SOA. This is because the coherent population oscillation technique can easily be implemented at room temperature and has a simple structure. The parameters of the SOA, such as the modulation frequency of the injected current, the magnitude of the direct current, the relative phase of the modulated current, the linewidth enhancement factor of the SOA, and the facet-face reflectivity, are all analyzed to reflect the effect of the SOA parameters on the modulation of the SFL effect from the phase delay.

2. The theoretical model

We consider a current-driven SOA, assuming that the injected light signal consists of a direct current control light signal E_0 and two sideband light signals E_1 and E_{-1}, depicted in Fig. 1. The amplification and absorption characteristics of the semiconductor medium can be achieved at a relatively low injection current by regulating the injection current of the SOA.

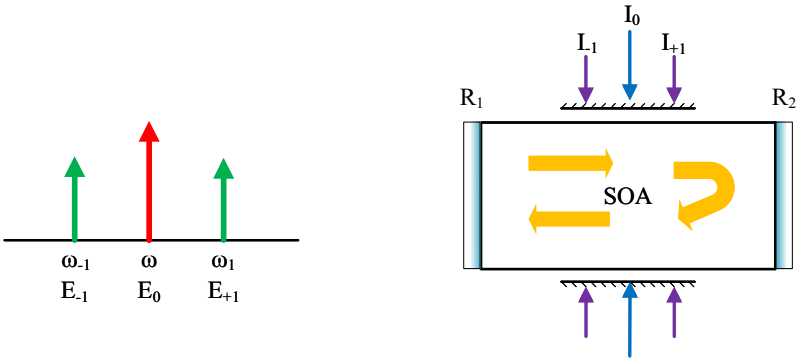

Fig. 1. Current-modulated SOA and the spectral components of the injected optical field (angular frequency of the sidebands shift from ω by δ: $\omega_{\pm 1} = \omega \pm \delta$).

The reflectivity of the front and the rear-facet of the SOA are taken as R_1 and R_2 to simulate the propagation of the light field in a semiconductor. One needs to consider the case where the light beam $\varepsilon^{\pm}(t)$ hits the medium. The light field can be shown as follows [10, 11]:

$$\varepsilon^{\pm}(t) = \frac{1}{2}E^{\pm}(t)\exp(-i\omega t) + \text{c.c.} \tag{1}$$

Here is the angular frequency of the optical field and $E^{\pm}(t)$ is the slowly varying amplitude. In this article, the superscript "+" indicates a light field transmitted forward, and the superscript "–" indicates a light field transmitted backward. Assume that the field is composed of a strong control beam $E_0^{\pm}$ and two sidebands $E_1^{\pm}$ and $E_{-1}^{\pm}$. Then the expression $E^{\pm}(t)$ can be shown as follows:

$$E^{\pm}(t) = E_0^{\pm}(t) + E_1^{\pm}(t)\exp(-i\delta t) + E_{-1}^{\pm}(t)\exp(i\delta t) \tag{2}$$

The three components of the electric field interact with the carriers in the semiconductor through the simulated emission when this modulated beam passes through the SOA. The modulation of the carrier concentration enables the creation of frequency beat between optical waves. The carriers in the semiconductor can follow the oscillation between the conduction and valence bands when the beating frequency is sufficiently small, generating a temporal grating and initiating an energy exchange between the control and sideband fields. The rate equation of carrier density N is:

$$\frac{\mathrm{d}N}{\mathrm{d}t} = \frac{I}{qV} - \frac{N}{\tau} - \frac{1}{2}n_{\mathrm{bg}}c\varepsilon_0\frac{\Gamma g(N)}{\hbar\omega_0}\langle|E^{+}(t)|^2 + |E^{-}(t)|^2\rangle \tag{3}$$

Here I is the injection current, q is the electron charge, V is the volume of the active region, Γ is the light field confinement factor, ω_0 is the angular frequency, $\hbar$ is Planck constant, τ is the carrier lifetime, c is the speed of light in vacuum, n_{bg} is the background refractive index of the material, ε_0 is the permittivity in free space, and $g(N)$ is the mode gain which can be represented as follows:

$$g(N) = \alpha(N - N_{\mathrm{t}}) \tag{4}$$

Here α is the differential gain coefficient, and N_{t} is the transparent carrier concentration in the active region.

In the study of SFL performance in the SOA, the optical beam and the bias current are modulated at the same frequency. By modulating the bias current to generate oscillations, the bias current and carrier density can be described as follows:

$$I(t) = I_0 + I_{+1}\exp[-i(\delta t - \psi)] + I_{-1}\exp[i(\delta t - \psi)] \tag{5}$$

$$N = N_0 + N_{-1}\exp(i\delta t) + N_1\exp(-i\delta t) \tag{6}$$

Here, I_0 is the direct current, $I_{\pm 1}$ is the modulation current, and ψ is the relative phase. We assuming that the modulation of the detection light field can be expressed and controlled by the phase of the modulation current, and that the current is independent of the spatial coordinates. Next, N_0 is the static carrier density and $N_{\pm 1}$ is the amplitude of the carrier population oscillation of the corresponding sideband. The three components of the electric fields interact with each other and cause a relative phase shift when the modulated beam passes through the SOA. The interaction of the sidebands and the control beam produces a coherent population oscillation effect, which results in changes in the temporal refractive index and the group velocity of the light signal; thus, producing a phase shift [12, 13].

For solving Eq. (3), the expressions for $E(t)$, $g(N)$ and $I(t)$ are substituted into Eq. (3) to obtain the following equation:

$$\begin{aligned}\frac{\mathrm{d}N}{\mathrm{d}t} = & -\frac{N}{\tau}+\frac{N_\mathrm{t}}{\tau}\left\{R'_0+R'_1\exp\left[-i(\delta t-\psi)\right]+R'_{-1}\exp\left[i(\delta t-\psi)\right]\right\} \\ & -\frac{(N-N_\mathrm{t})}{\tau P_\mathrm{s}}\frac{1}{2}n_{\mathrm{bg}}c\varepsilon_0\Big[\left|E_0^+\right|^2+(E_0^{+*}E_1^+ + E_0^+E_{-1}^{+*})\exp(-i\delta t) \\ & \qquad +(E_0^+E_1^{+*}+E_0^{+*}E_{-1}^+)\exp(i\delta t)\Big] \\ & -\frac{(N-N_\mathrm{t})}{\tau P_\mathrm{s}}\frac{1}{2}n_{\mathrm{bg}}c\varepsilon_0\Big[\left|E_0^-\right|^2+(E_0^{-*}E_1^- + E_0^-E_{-1}^{-*})\exp(-i\delta t) \\ & \qquad +(E_0^-E_1^{-*}+E_0^{-*}E_{-1}^-)\exp(i\delta t)\Big] \end{aligned} \tag{7}$$

Where the following normalized currents $R'_{0,\pm 1}$ and power P_s are defined as:

$$R'_{0,\pm 1} = \frac{\tau}{qVN_\mathrm{t}}I_{0,\pm 1} \tag{8}$$

$$P_\mathrm{s} = \frac{\hbar\omega_0}{\Gamma\alpha\tau} \tag{9}$$

It is assumed that there is no interaction between the forward-transmitted and back -transmitted light signals. The slowly varying envelope approximation of the propagation equation is:

$$\frac{\mathrm{d}E^\pm}{\mathrm{d}z} = \frac{1}{2}g(N)(1-i\beta)E^\pm \tag{10}$$

where β is the linewidth enhancement factor.

The expressions for $g(N)$, $N(t)$ and $E^\pm(t)$ are substituted into Eq. (10) to obtain the following equation:

$$\frac{\mathrm{d}E^{\pm}}{\mathrm{d}z} = \frac{1}{2}(1-i\beta)\alpha N_{\mathrm{t}}\left[\frac{N_0}{N_{\mathrm{t}}} - 1 + \frac{N_{-1}}{N_{\mathrm{t}}}\exp(i\delta t) + \frac{N_1}{N_{\mathrm{t}}}\exp(-i\delta t)\right]$$
$$\times\left[E_0^{\pm}(t) + E_1^{\pm}(t)\exp(-i\delta t) + E_{-1}^{\pm}(t)\exp(i\delta t)\right]$$
$$= \frac{\partial E_0^{\pm}}{\partial z} + \frac{\partial E_{-1}^{\pm}}{\partial z}\exp(i\delta t) + \frac{\partial E_1^{\pm}}{\partial z}\exp(-i\delta t) \tag{11}$$

After rectifying the Eq. (11), equations for the propagation of the optical field are given by:

$$\frac{\partial E_0^{\pm}}{\partial z} = \frac{1}{2}(1-i\beta)\alpha N_{\mathrm{t}}\left[\left(\frac{N_0}{N_{\mathrm{t}}} - 1\right)E_0^{\pm} + \frac{N_1}{N_{\mathrm{t}}}E_{-1}^{\pm} + \frac{N_{-1}}{N_{\mathrm{t}}}E_1^{\pm}\right] \tag{12a}$$

$$\frac{\partial E_1^{\pm}}{\partial z} = \frac{1}{2}(1-i\beta)\alpha N_{\mathrm{t}}\left[\left(\frac{N_0}{N_{\mathrm{t}}} - 1\right)E_1^{\pm} + \frac{N_1}{N_{\mathrm{t}}}E_0^{\pm}\right] \tag{12b}$$

$$\frac{\partial E_{-1}^{\pm}}{\partial z} = \frac{1}{2}(1-i\beta)\alpha N_{\mathrm{t}}\left[\left(\frac{N_0}{N_{\mathrm{t}}} - 1\right)E_{-1}^{\pm} + \frac{N_{-1}}{N_{\mathrm{t}}}E_0^{\pm}\right] \tag{12c}$$

At the same time, differentiating for t in Eq. (6) gives:

$$\frac{\mathrm{d}N}{\mathrm{d}t} = \frac{\mathrm{d}N_0}{\mathrm{d}t} + i\delta N_{-1}\exp(i\delta t) - i\delta N_1\exp(-i\delta t) \tag{13}$$

Combining Eqs. (7) and (13) gives:

$$\frac{N_0}{N_{\mathrm{t}}} = \frac{R_0' + q_0}{1 + q_0} \tag{14a}$$

$$\frac{N_1}{N_{\mathrm{t}}} = \frac{R_1'\exp(i\psi) - (N_0/N_{\mathrm{t}} - 1)q_{\mathrm{t}}}{1 + q_0 - i\delta\tau} \tag{14b}$$

$$\frac{N_{-1}}{N_{\mathrm{t}}} = \left(\frac{N_1}{N_{\mathrm{t}}}\right)^* \tag{14c}$$

Using (12) and (14), the following set of equations for the amplitudes of the optical fields are obtained:

$$\frac{\partial E_0^{\pm}}{\partial z} = \frac{\alpha N_{\mathrm{t}}(1-i\beta)}{2\omega_{\mathrm{c}}}\left[(R_0' - 1)E_0^{\pm} + \frac{\omega_{\mathrm{c}}R_1'\exp(i\psi) - (R_0' - 1)q_1}{\omega_{\mathrm{c}} - i\delta\tau}E_{-1}^{\pm}\right.$$
$$\left. + \frac{\omega_{\mathrm{c}}R_1'\exp(-i\psi) - (R_0' - 1)q_1^*}{\omega_{\mathrm{c}} + i\delta\tau}E_1^{\pm}\right] \tag{15a}$$

$$\frac{\partial E_1^{\pm}}{\partial z} = \frac{\alpha N_t(1-i\beta)}{2\omega_c}\left[(R_0'-1)E_1^{\pm} - \frac{(R_0'-1)q_1}{\omega_c - i\delta\tau}E_0^{\pm} + \frac{\omega_c R_1' \exp(i\psi)}{\omega_c - i\delta\tau}E_0^{\pm}\right] \tag{15b}$$

$$\frac{\partial E_{-1}^{\pm}}{\partial z} = \frac{\alpha N_t(1-i\beta)}{2\omega_c}\left[(R_0'-1)E_{-1}^{\pm} - \frac{(R_0'-1)q_1^*}{\omega_c + i\delta\tau}E_0^{\pm} + \frac{\omega_c R_1' \exp(-i\psi)}{\omega_c + i\delta\tau}E_0^{\pm}\right] \tag{15c}$$

Among them, the normalized optical powers are defined as follows:

$$q_0 = \frac{1}{2} n_{bg} c\varepsilon_0 \frac{\left|E_0^+\right|^2 + \left|E_0^-\right|^2}{P_s} \tag{16}$$

$$q_1 = \frac{1}{2} n_{bg} c\varepsilon_0 \frac{E_0^{+*}E_1^+ + E_0^+E_{-1}^{+*} + E_0^{-*}E_1^- + E_0^-E_{-1}^{-*}}{P_s} \tag{17}$$

In Equation (15), $\omega_c = 1 + q_0$. For SFL in semiconductor waveguides, the group refractive index is generally used as a measurement parameter:

$$v_g = \frac{c}{n_g}, \quad n_g = n_{bg} + \frac{dn_{bg}}{d\omega}\omega = n_{bg} + \Delta n_g \tag{18}$$

Here n_g is the group refractive index, and v_g is the group velocity of the waveguide. It can be seen that the group velocity is inversely proportional to the group refractive index. The group refractive index consists of two parts: the intrinsic refractive index of the material n_{bg}, and the change in the refractive index caused due to effects such as coherent population oscillations Δn_g. While the change in refractive index can be reflected by the phase delay [14]:

$$\Delta n_g = \frac{c}{L}\Delta t = \frac{c}{L}\frac{\Delta\varphi}{\delta} \tag{19}$$

Here Δt is the length of the transmission time, L is the length of the waveguide, and $\Delta\varphi$ is the phase delay of the light wave. In Eq. (19), we can see that the change in the refractive index of the group is proportional to the phase change, which implies that the slow-fast light effects can be measured by phase delays on the light signal envelope. The SFL effect would be detected by the amplitude and phase of the modulated signal E_1.

All equations in the model are solved by using a numerical simulation. The SOA is divided into many equal sections to find the carrier density for each section. The optical signals are varied along the forward and backward propagating directions. The reflected and transmitted optical fields at the end face are calculated according to the reflectivity R_1 and R_2. The photon concentration and phase are calculated for each section.

3. Results of simulations

Based on the numerical model of this paper, this section discusses the effect of the facet-reflection-based SOA parameters on the SFL. The design on facets reflections may include two coating schemes, reflective coating on two facets or AR coating on the front-facet and reflection coating on the rear-facet. The optical field limiting factor Γ is 0.5 in the numerical model. The active carrier lifetime τ is 300 ps. The length L of the SOA is 0.3 mm. The gain coefficient is $\alpha = 3 \times 10^{-20}$ m^2. The transparent carrier density is $N_t = 1 \times 10^{18}$ cm^{-3}. The background refractive index of the material is $n_{bg} = 3.2$.

The phase delay variation of the forward output signal with modulation frequency in the case of the parameter linewidth enhancement factor $\beta = 0$, the injection currents $I_0 = 100$ mA, and $I_{+1} = I_{-1} = 10$ mA, is shown in Fig. 2. Here, the solid line is the curve E_1 and the dashed line is the curve E_{-1} that are filtered out using optical filters. These two curves have a symmetrical shape since the sideband signal transmission equation in Eq. (15) is conjugate, leading to the phase being opposite. The second term of the Eq. (15) on the right side of the equation reflects the four-wave mixing effect. The coherent population oscillation generates the slow light and fast light phenomenon due to the four-wave mixing effect. We get the maximum value of the phase delay when $\beta = 0$, the phase delay is proportional to $\delta\tau/(\omega_c^2 + (\delta\tau)^2)$, and when $\omega_c = \delta\tau$ resonance is generated.

There is a control beam optical power of 15 mW and a sideband optical power of 10 mW injection, and the phase delay of the forward transmission signal varies with the modulation frequency for different direct currents as shown in Fig. 3. It can be seen that by increasing the modulation frequency, the phase delay tends to increase first and then decreases; the maximum phase delay is near 1 GHz. The maximum phase delay shows a gradually decreasing trend, and the phase delay changes from a positive to a negative value when a larger direct current is injected.

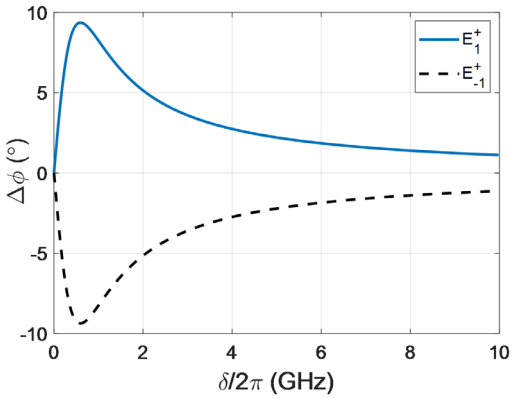

Fig. 2. Variation of phase delay with modulation frequency.

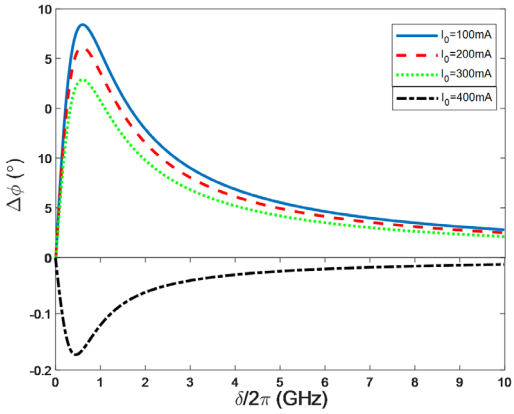

Fig. 3. For different direct currents, the phase delay varies with the modulation frequency.

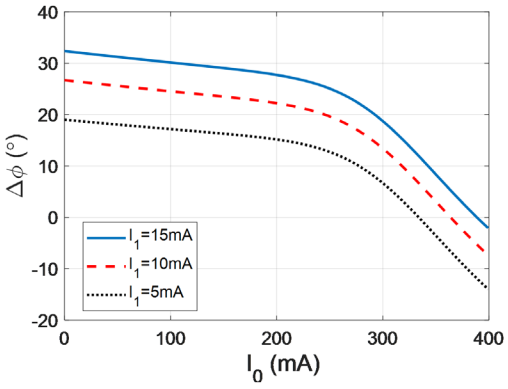

Fig. 4. For different input modulation currents, the phase delay varies with the magnitude of the direct current.

Figure 4 shows the variation of the phase delay with the direct current magnitude for different input modulation currents. It can be seen that as the injected control beam becomes larger, the phase delay tends to become smaller. At the same direct current, the phase delay becomes larger as the input modulating current increases. The transparent current is also different for different modulating currents. As the modulating current increases, the transparent current also increases. The phase delay is positive when the input direct current is less than the transparent current; then, the slow light is obtained. Also, when the input of direct current is greater than the transparent current, the phase delay is negative, implying that the obtained light is fast.

The light signal is in the absorption region, the optical power in the SOA gradually decreases from the front-facet to the rear-facet, and the phase delay is positive, which means that the slow light is obtained when the direct current input is smaller than the transparent transmission current as shown in Fig. 5(a). The light signal remains in the

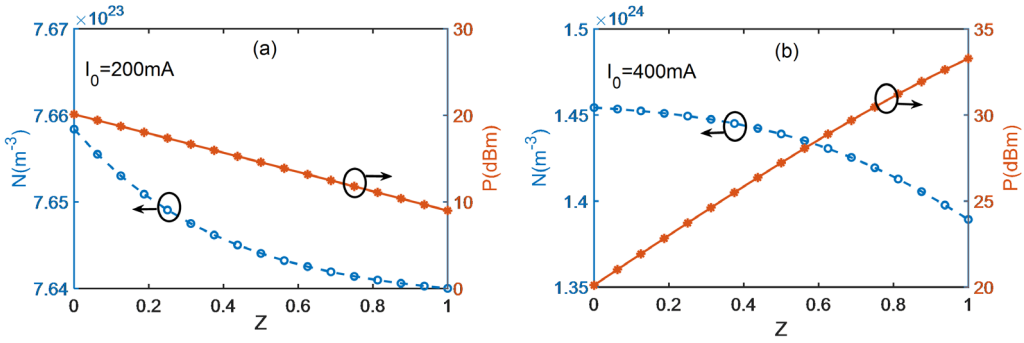

Fig. 5. Steady-state carrier density and optical power distribution in SOAs.

gain area, the optical power gradually increases from the front-facet to the rear-facet, the phase delay is negative, which means that the fast light is obtained when the input direct current is larger than the transparent transmission current, as shown in Fig. 5(b).

The phase delay of the control beam signal and the sideband light signal varies with the modulation frequency for different linewidth enhancement factors, as shown in Fig. 6. The phase delay of the control beam signal is equal to 0 when the linewidth enhancement factor $\beta = 0$, and it does not change with the modulation frequency. The two sideband light signals display a symmetric phase change correlation. Overall, the phase delay of the control beam signal and the two sideband light signals are moved up when the linewidth enhancement factor is not equal to 0. The control beam signal is no longer 0, and the phase delay for both the sideband light signals is no longer a symmetric correlation. Additionally, the phase delay of the signal light E_{-1} changes from negative to positive. This means that the sideband signal light changes from fast light to slow light.

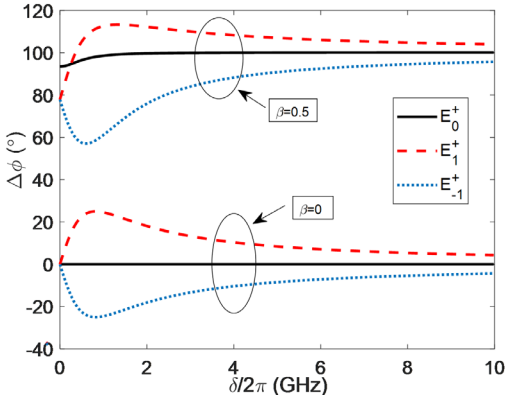

Fig. 6. Variation of the phase delay with modulation frequency for different linewidth enhancement factors for light signals E_0, E_1 and E_{-1} (black solid line for E_0, red dashed line and blue dotted line for E_1 and E_{-1}, separately).

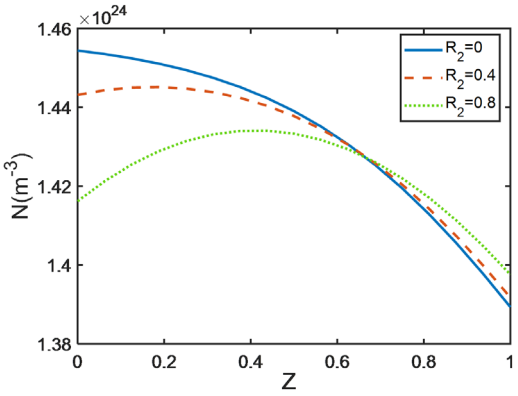

Fig. 7. For different rear-facet reflectivity, the distribution of steady-state carrier density in SOAs.

In the following analysis, the linewidth enhancement factor is set equal to 0 and the modulating current size is set to 10 mA for analyzing the effect of the facet reflectivity on the fast and slow light. From Fig. 7, it can be seen that the facet reflectivity has a larger impact on the front-facet steady-state carrier density. The larger the rear -plane reflectivity, the more would be the light signal reflected, leading to a larger concentration of photon numbers at the front-facet. The higher the photon concentration, the more carriers in the active region may be consumed. As a consequence, the carrier density of the front-facet in the SOA with large rear-facet reflectivity is smaller than that in the SOA with small rear-facet reflectivity.

In the case of the front-facet reflectivity $R_1 = 0$, which is obtained by slow light, the phase delay of the forward output signal with modulation frequency is given, as shown in Fig. 8(a). We can see that the maximum phase delay decreases with the increase of the reflectivity at the rear-facet. In the case of fast light, the change of the output phase delay is given, as shown in Fig. 8(b). At this point, the peak value of the phase delay

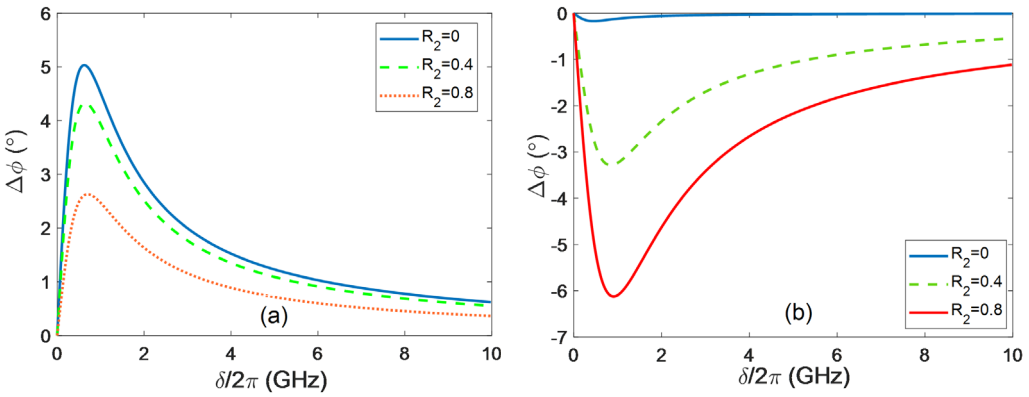

Fig. 8. For different rear-facet reflectivity, the phase delay varies with modulation frequency.

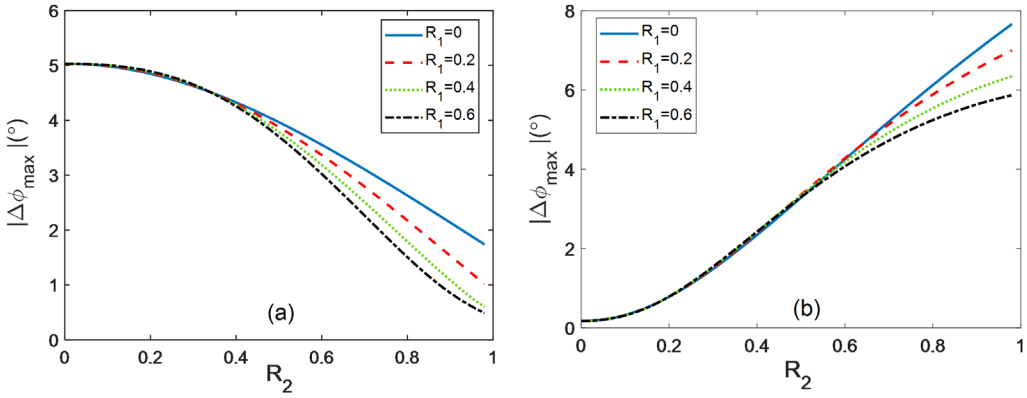

Fig. 9. For different front-facet reflectivities, the variation of the maximum phase delay with the magnitude of the rear-facet reflectivity.

increases with an increase in the reflectivity of the rear-facet. It could be seen that the fast-slow light effect can be influenced by the size of the rear-facet reflectivity.

In the case of different front-facet reflectivity, the obtained curve of the phase delay variation varies with the magnitude of the rear-facet reflectivity, as shown in Fig. 9. The maximum phase delay variation works from the curve of phase delay change with the modulation frequency. The input current setting is smaller than the transparent transmission current, as shown in Fig. 9(a). Therefore, the obtained phase delay is positive; thus, obtaining the case of slow light. From the figure, it can also be observed that the obtained maximum phase delay variation gradually becomes smaller as the rear-facet reflectivity becomes larger. At the same time, the difference of the phase delay obtained from different front-facet reflectivity is not noticeable when the reflectivity of the rear-facet is small. In the large reflectivity of the rear-facet, the phase delay decreases as the reflectivity of the front-facet increases. The input current setting is larger than the transparent transmission current, as shown in Fig. 9(b). The case of fast light is obtained, and the obtained phase delay is completely negative. From the figure, it can be seen that the obtained maximum phase delay variation gradually becomes larger as the rear-facet reflectivity increases. A larger maximum phase delay variation can be obtained when the front-facet reflectivity is small. Therefore, in the slow light area, when the rear-facet reflectivity is small, a larger phase delay variation can be obtained. While in the fast light area, a larger variation of phase delay can be obtained when the rear-facet reflectivity is large.

The phase delay of the light signal with the relative phase of the modulating current for different rear-facet reflectivity is shown in Fig. 10. From the figure, it can be observed that the phase delay shows a sine wave-like variation pattern as the relative phase increases. The phase delay curve is symmetric, $\Delta\varphi = 0$. The variation of the curve gradually decreases when the reflectivity of the rear-facet gradually increases. Meanwhile, changing the relative phase allows the signal to switch between the SFL. These

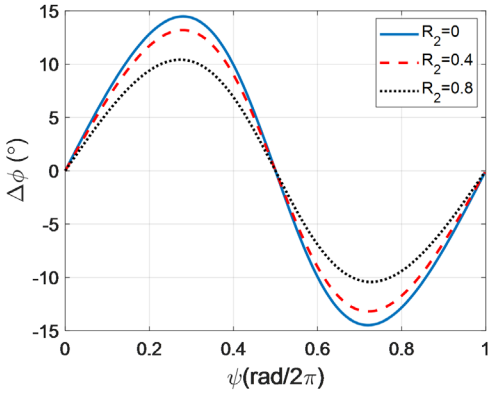

Fig. 10. For different rear-facet reflectivity, the phase delay of the light signal varies with the relative phase of modulating current.

analyses are beneficial to us for using the device parameters in the SOA to adjust the SFL. Enhanced signal processing can be performed using both the SFL.

4. Conclusion

In this paper, a numerical analysis model of the fast and slow light effects caused due to the nonlinear effects of coherent population oscillations in facet-reflectivity SOA is constructed. The importance of higher-order nonlinear effects of the facet-reflectivity SOA on the interaction between light and matter is demonstrated in this study. The phase delay can be altered by adjusting the parameters of current modulation frequency, the magnitude of direct current, and the rear-facet reflectivity in the SOA, thereby demonstrating that the fast and slow light effects in the SOA can be controlled by these parameters. When the direct current is small, it is more effective to use the magnitude of the direct current to adjust the phase delay of the SFL. A larger phase delay can be obtained when the modulation current is higher, and the modulation frequency is near 1 GHz. In addition, for slow light, the larger the facet-reflectivity, the smaller would be the change in phase delay. For fast light, the larger the facet-reflectivity, the larger would be the change in phase delay.

Acknowledgements
This work is supported by the Natural Science Foundation of Jiangsu Province (BK20191012).

References

[1] XINHAI ZOU, SHANGJIAN ZHANG, HENG WANG, ZHIYAO ZHANG, JINJIN LI, YALI ZHANG, SHUANG LIU, YONG LIU, *Microwave photonic harmonic down-conversion based on cascaded four-wave mixing in a semiconductor optical amplifier*, IEEE Photonics Journal **10**(1), 2018, article no. 5500308, DOI: 10.1109/JPHOT.2017.2785409.

[2] Wenhui Zhan, Peng Zhou, Yuxiao Zeng, Masaru Mukaikubo, Takuo Tanemura, Yoshiaki Nakano, *Optimization of modulation canceling reflective semiconductor optical amplifier for colorless WDM transmitter applications*, Journal of Lightwave Technology **35**(2), 2017, pp. 274–279, DOI: 10.1109/JLT.2016.2633719.

[3] Qin J., Lu G.-W., Sakamoto T., Akahane K., Yamamoto N., Wang D., Wang C., Wang H., Zhang M., Kawanishi T., Ji Y., *Simultaneous multichannel wavelength multicasting and XOR logic gate multicasting for three DPSK signals based on four-wave mixing in quantum-dot semiconductor optical amplifier*, Optics Express **22**(24), 2014, pp. 29413–29423, DOI: 10.1364/OE.22.029413.

[4] Zajnulina M., Lingnau B., Lüdge K., *Four-wave mixing in quantum-dot semiconductor optical amplifiers: a detailed analysis of the nonlinear effects*, IEEE Journal of Selected Topics in Quantum Electronics **23**(6), 2017, article no. 3000112, DOI: 10.1109/JSTQE.2017.2681803.

[5] Sun D., Ku P.C., *Slow light using p-doped semiconductor heterostructures for high-bandwidth nonlinear signal processing*, Journal of Lightwave Technology **26**(23), 2008, pp. 3811–3817, DOI: 10.1109/JLT.2008.2005121.

[6] Kohandani R., Zandi A., Kaatuzian H., *Analysis of the effects of applying external fields and device dimensions alterations on GaAs/AlGaAs multiple quantum well slow light devices based on excitonic population oscillation*, Applied Optics **53**(6), 2014, pp. 1228–1236, DOI: 10.1364/AO.53.001228.

[7] Trines R.M.G.M., Alves E.P., Webb E., Vieira J., Fiúza F., Fonseca R.A., Silva L.O., Cairns R.A., Bingham R., *New criteria for efficient Raman and Brillouin amplification of laser beams in plasma*, Scientific Reports **10**, 2020, article no. 19875, DOI: 10.1038/s41598-020-76801-z.

[8] Xiao-Jun Zhang, Hai-Hua Wang, Lei Wang, Jin-Hui Wu, *Optically tunable gratings based on coherent population oscillation*, Scientific Reports **8**(1), 2018, article 6834, DOI: 10.1038/s41598-018-25010-w.

[9] Chang S.W., Kondratko P.K., Su H., Chuang S.L., *Slow light based on coherent population oscillation in quantum dots at room temperature*, IEEE Journal of Quantum Electronics **43**(2), 2007, pp. 196–205, DOI: 10.1109/JQE.2006.889060.

[10] Duill S.O., O'Dowd R.F., Eisenstein G., *On the role of high-order coherent population oscillations in slow and fast light propagation using semiconductor optical amplifiers*, IEEE Journal of Selected Topics in Quantum Electronics **15**(3), 2009, pp. 578–584, DOI: 10.1109/JSTQE.2009.2013177.

[11] Antón M.A., Carreño F., Calderón Ó.G., Melle S., Arrieta-Yáñez F., *Phase-controlled slow and fast light in current-modulated semiconductor optical amplifiers*, Journal of Physics B: Atomic, Molecular and Optical Physics **42**(9), 2009, article no. 095403, DOI: 10.1088/0953-4075/42/9/095403.

[12] Uskov A.V., Sedgwick F.G., Chang-Hasnain C.J., *Delay limit of slow light in semiconductor optical amplifiers*, IEEE Photonics Technology Letters **18**(6), 2006, pp. 731–733, DOI: 10.1109/LPT.2006.871147.

[13] Gallo K., Assanto G., *All-optical diode based on second-harmonic generation in an asymmetric waveguide*, Journal of the Optical Society of America B **16**(2), 1999, pp. 267–269, DOI: 10.1364/JOSAB.16.000267.

[14] Shumakher E., Duill S.O., Eisenstein G., *Optoelectronic oscillator tunable by an SOA based slow light element*, Journal of Lightwave Technology **27**(18), 2009, pp. 4063–4068, DOI: 10.1109/JLT.2009.2022045.

Received April 14, 2022
in revised form June 20, 2022